Formation Process of Three-Dimensional Arrays from Silica Spheres

Keiji Ishikawa, Hironori Harada, and Tatsuya Okubo
Dept. of Chemical System Engineering, The University of Tokyo, Tokyo 113-8656, Japan

Elucidating the formation process of 3-D arrays from submicrometer-sized particles is a key to creating an optimal fabrication process of photonic crystals. In this research, the spontaneous sedimentation of silica spheres is imaged by in situ confocal laser scanning microscopy, and the dynamics is studied. When the pH is 7.0 and 10, the rate of the formation process of a hexagonal structure is attributed to the transport of spheres in the early stage of precipitation, and can be reproduced by a simple equation for Langmuir-type adsorption, ignoring the desorption part. In a later stage, however, the rate becomes smaller. In the first layer, even after drying, the nearest two spheres are separated, while maintaining a hexagonal structure. From the results, the formation process of three-dimensional arrays from silica spheres is illustrated.

Introduction

Photonic crystals with periodic structures on the order of the optical wavelength have attracted considerable attention, because they can manipulate the propagation of photons in all three directions, and are expected to be applicable to various optical systems (Yablonovitch, 1987; John, 1987; Joannopoulos et al., 1995). Fabrication methods based on self-assembly, in which building blocks are spontaneously organized into stable, well-defined structures, are promising for industrial uses (Xia et al., 2000), and many processes have been proposed, such as spontaneous sedimentation (Bogomolov et al., 1997; Míguez et al., 1997), electrophoretic deposition (Holgado et al., 1999; Rogach et al., 2000), and filtration (Park et al., 1998). It is still impossible to fabricate large-size ordered structures within a short time, or manipulate the defects at prescribed positions within the crystals, because the formation process of three-dimensional (3-D) arrays is not well understood.

There have been some studies on the formation process of particle arrays. Nagayama and coworkers observed the formation of 2-D latex-particle arrays in the drying process, and showed that the dynamics of 2-D ordering were governed by the attractive capillary forces and the convective transport of particles toward the ordered region (Denkov et al., 1992; Dimitrov and Nagayama, 1996). 3-D arrays of particles in concentrated suspensions are known as colloidal crystals and investigated experimentally (Pusey and van Megen, 1986; Yoshida et al., 1991) and theoretically (Ackerson and Schatzel, 1995; Harland and van Megen, 1997). Still, the dynamics of the formation process of 3-D arrays as well as the drying process afterward have not been well understood.

In this study, the spontaneous sedimentation of silica spheres was imaged by *in situ* confocal laser scanning microscopy during and after the sedimentation, as well as before and after the drying stage, and the dynamics of the formation process of 3-D arrays were analyzed and modeled.

Experimental

Silica spheres whose diameters were 700 nm, 1,000 nm, and 1,500 nm were provided by Nippon Shokubai Co., Ltd. These samples were monodispersed silica spheres with polydispersity less than 5% established by dynamic light scattering (DLS: Otsuka Electronics Co., Ltd, ELS-8000). Silica spheres were dispersed in water purified by a Milli-Q system (Millipore). HClaq and NaOH (WAKO) were added to control the pH. The zeta potential of the silica-spheres dispersion was measured by electrophoretic light scattering (ELS: Otsuka Electronics Co., Ltd, ELS-8000).

To visualize the dynamics of the silica spheres in the spontaneous sedimentation, a confocal laser scanning microscope (Leica Microsystems, TCS NT) was used. The suspension of silica spheres was poured into glass-bottom microwell dishes (MatTek Co., P35G-0-10-C-gm), and silica spheres were deposited on a cover glass substrate by the force of gravity. The

Correspondence concerning this article should be addressed to T. Okubo

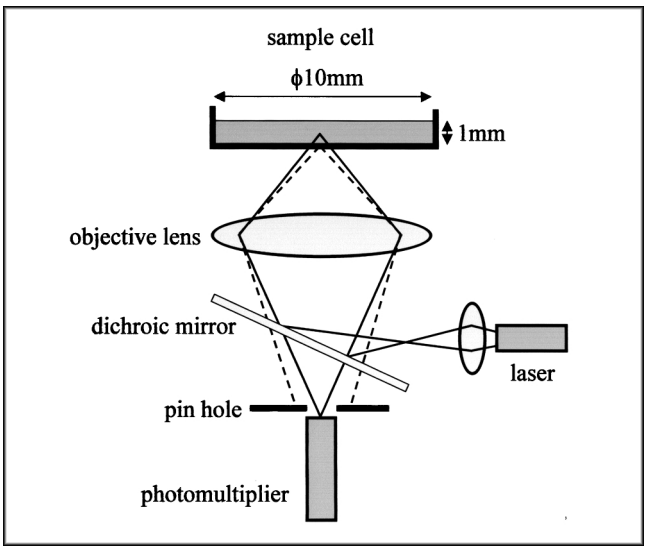

Figure 1. Experimental apparatus.

size of the substrate was ϕ10 mm in diameter, and the poured suspension was 1 mm high. Silica spheres were observed *in situ* from the bottom through the cover glass substrate by the confocal laser scanning microscope during and after the spontaneous sedimentation, as shown in Figure 1. After the sedimentation was completed, the suspension was dried in an incubator at 313 K, and the silica spheres thus obtained were described.

In this observation, the flux of silica spheres by number and the pH of the suspension were changed, and the first and the second layers on the substrate were observed *in situ*. The flux, f, was calculated as the product of the measured concentration by number, C, and the sedimentation velocity, v, determined by Stokes' law

$$f = Cv \tag{1}$$

$$v = \frac{\rho_s - \rho_w}{18\eta} d^2 g \tag{2}$$

where ρ_s and ρ_w are the mass densities of the silica sphere and water, respectively, η is the viscosity of water, d is the diameter of the silica spheres, and g is the gravitational acceleration. The sedimentation velocity was measured independently in each size of the silica spheres, and the validity of Stokes' law was confirmed.

Results

The photographs taken by the confocal laser scanning microscopy were processed as follows. First, circles were drawn with silica spheres for their centers. Next, the number of circles in the unit area was counted. For quantitative consideration and comparison of each photograph, the filling factor and the radial distribution function (RDF) were introduced. The observed area in each condition was 25 μm $\times$25 μm.

The filling factor, θ, denotes the ratio of the area occupied by these per unit area. The filling factor is defined by the

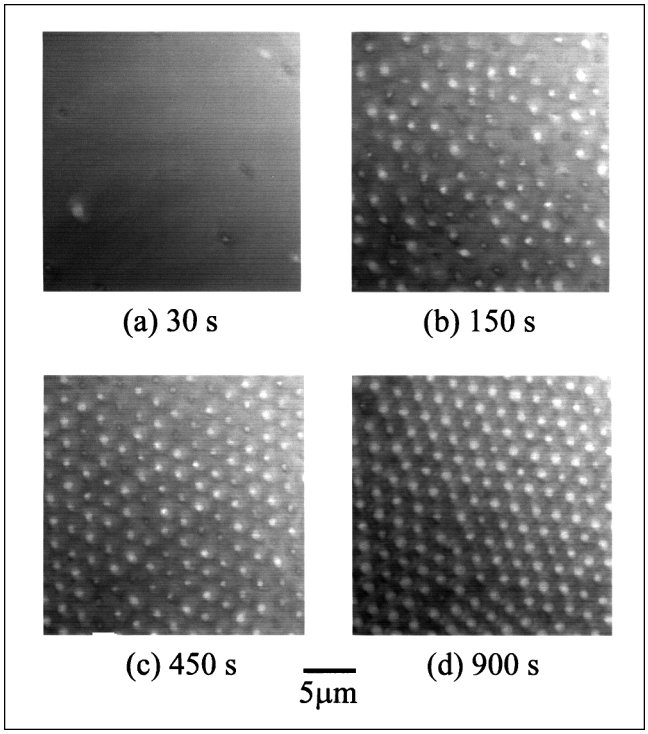

Figure 2. First layer observed by a confocal laser scanning microscope.

Diameter of silica spheres is 1,500 nm and the flux is 1.1×10^9 spheres $m^{-2}\cdot s^{-1}$.

following equation

$$\theta = \frac{\pi N d^2}{4} \tag{3}$$

where N denotes the number of circles in the unit area. If silica spheres are in direct contact and are packed hexagonally, the filling factor should equal the maximum value, 0.907.

The RDF is calculated by counting all distances between the centers of any two circles in a photograph. If the silica spheres are arranged in a regular structure, periodic peaks should be observed.

Figure 2 shows examples of the photographs taken by the confocal laser scanning microscope, where the diameter of the silica spheres is 1,500 nm, the flux is 1.1×10^9 spheres $m^{-2}\cdot s^{-1}$, and the pH is 7.0.

Figure 3 shows the RDFs of the first layer of silica spheres on the substrate when the diameter is 1,500 nm, the flux of the silica spheres is 1.1×10^9 spheres $m^{-2}\cdot s^{-1}$, and the pH is 7.0. While no peak is shown in the RDF at 150 s (Figure 3a), several peaks appear at 450 s (Figure 3b), which means that the silica spheres deposited on the substrate are gradually arranged into a regular structure. The first peak of the RDF at 450 s (Figure 3b) is shown at 2.0 μm, which corresponds to the distance between the nearest two spheres. The RDF given by the photograph at 900 s (Figure 3c) also shows similar peaks attributed to the regular arrangement, and the distance between the nearest two spheres is 1.9 μm. It was shown that the distance between the nearest two spheres de-

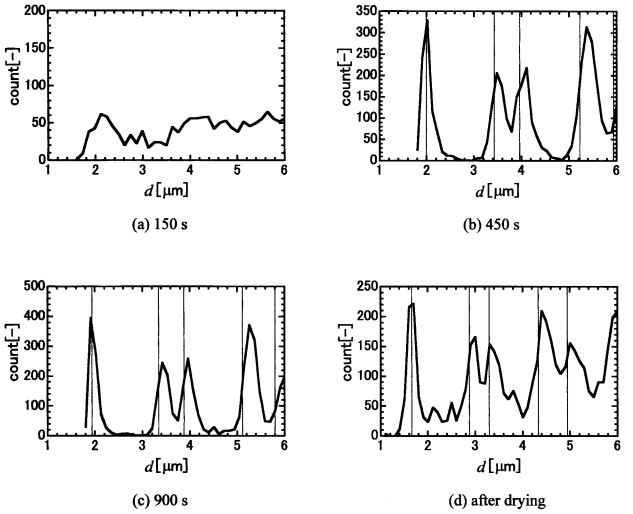

Figure 3. Changes in the RDF of the first layer with time.

The flux of the silica spheres is 1.1×10^9spheres $m^{-2}\cdot s^{-1}$. Vertical solid lines show the positions of periodic distances of two silica spheres attributed to the hexagonal structure.

creased, and the filling factor increased as silica spheres deposited on the first layer. In these steps, the silica spheres maintained a regular arrangement. The silica spheres did not come in direct contact with adjacent ones, and maintained a certain distance even after drying (Figure 3d). The smallest peak position in the RDF, which shows the distance between the nearest two spheres, is defined as d_n. The values for d_n, $\sqrt{3}\,d_n$ $2d_n$, $\sqrt{7}\,d_n$, 3 d_n are shown as vertical lines in Figure 3. When the spheres are arranged in a hexagonal structure, peaks in the RDF should be shown at the locations of the vertical lines. The values of the experimental peak positions

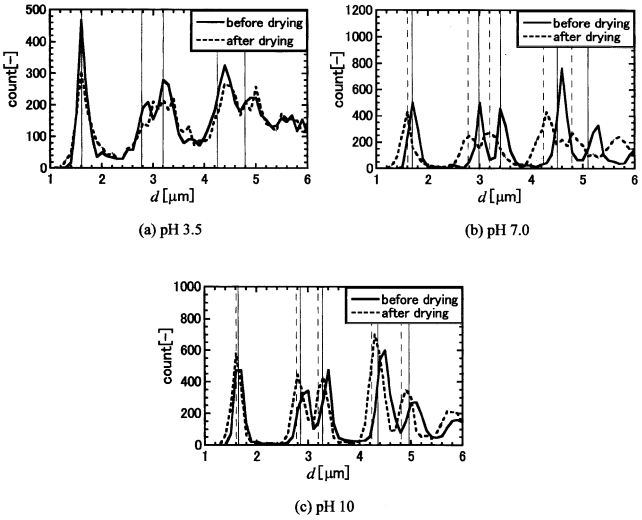

Figure 4. Changes in the RDF of the first layer with the pH before and after drying.

The diameter of silica spheres is 1,500 nm and the flux is 5.6×10^9 spheres $m^{-2}\cdot s^{-1}$. Vertical solid and dotted lines show the positions of periodic distances of two silica spheres attributed to the hexagonal structure before and after the drying, respectively.

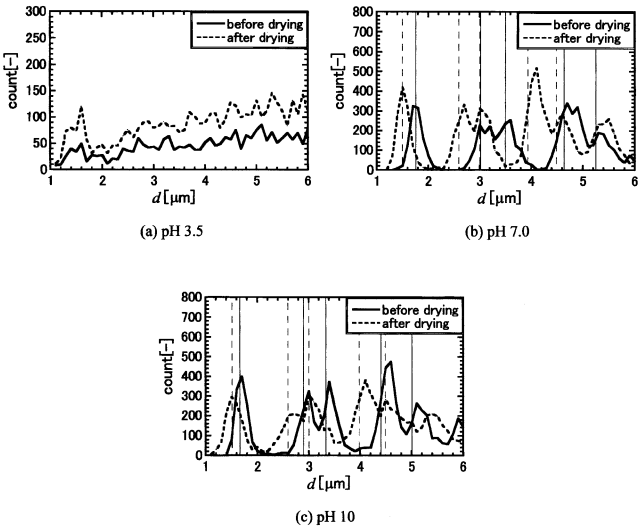

Figure 5. Changes in the RDF of the first layer with the pH before and after the drying.

The diameter of silica spheres is 1,000 nm and the flux is 5.6×10^9 spheres $m^{-2}\cdot s^{-1}$. Vertical solid and dotted lines show the positions of periodic distances of two silica spheres attributed to the hexagonal structure before and after the drying, respectively.

in Figure 3 are, however, somewhat larger than those vertical lines, due to some disorders in the hexagonal arrays.

Figures 4 and 5 show the changes in the RDFs of the first layer, with the pH before and after drying when the diameters are 1,500 nm and 1,000 nm, respectively. As for 700 nm, the RDFs of the first layer as a function of pH are shown in Figure 6 only before drying, because the silica sphere cannot be observed clearly and counted after drying. The flux is fixed at 5.6×10^9 spheres $m^{-2}\cdot s^{-1}$. When the pH is 3.5, near the isoelectric point, silica spheres aggregate, and do not settle

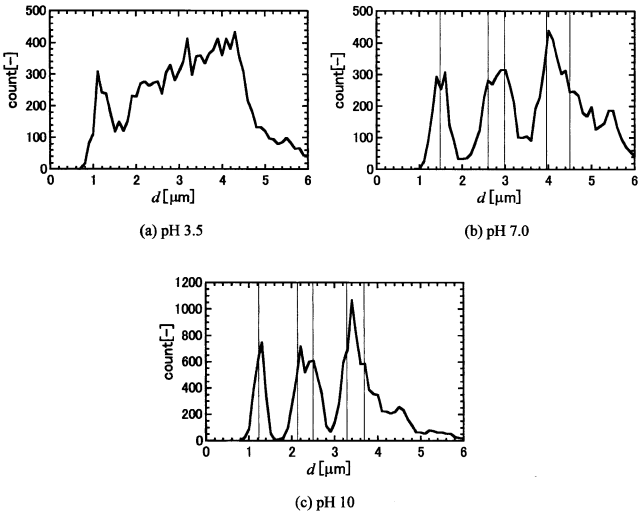

Figure 6. Changes in the RDF of the first layer with the pH before the drying.

The diameter of silica spheres is 700 nm and the flux is 5.6×10^9 spheres $m^{-2}\cdot s^{-1}$. Vertical solid lines show the positions of periodic distances of two silica spheres attributed to the hexagonal structure.

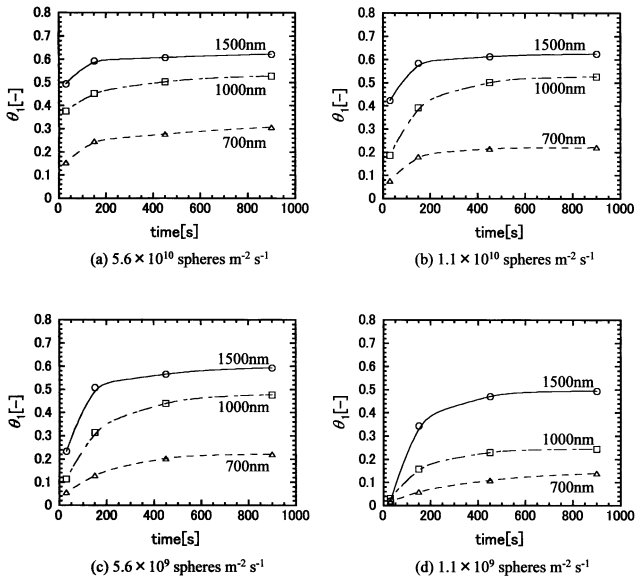

Figure 7. Changes in the filling factors of the first layer with time.

The fluxes of the silica spheres are (a) 5.6×10^{11} spheres $m^{-2}\cdot s^{-1}$; (b) 1.1×10^{10} spheres $m^{-2}\cdot s^{-1}$; (c) 5.6×10^{10} spheres $m^{-2}\cdot s^{-1}$, (d) 1.1×10^{9} spheres $m^{-2}\cdot s^{-1}$.

into a regular structure. The silica spheres settle at a pH of 7 or 10. As was the case in Figure 3, the peak positions in the RDF attributed to a hexagonal structure are shown in Figures 4–6.

Figure 7 shows the changes in the filling factors of the first layer on the substrate when the pH was 7.0, and the fluxes of the silica spheres were 5.6×10^{10}, 1.1×10^{10}, 5.6×10^{9} and 1.1×10^{9} spheres $m^{-2}\cdot s^{-1}$, respectively. In the early stage of sedimentation, the filling factor increases rapidly as the silica spheres precipitate. After this stage, the filling factor increased gradually and was saturated at a maximum value.

Figure 8 shows the changes in the filling factors of the second layer on the substrate when the diameter of the silica spheres was 1,500 nm, the pH was 7.0, and the fluxes were 1.1×10^{10} and 1.1×10^{9} spheres $m^{-2}\cdot s^{-1}$. The filling factors of the second layer on the substrate show a rapid increase during the early stage of sedimentation. In the later stage,

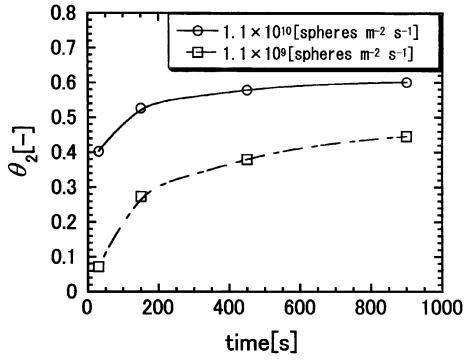

Figure 8. Changes in the filling factors of the second layer with time.

The diameter of silica spheres is 1,500 nm and the fluxes are 1.1×10^{10} and 1.1×10^{9} spheres $m^{-2}\cdot s^{-1}$.

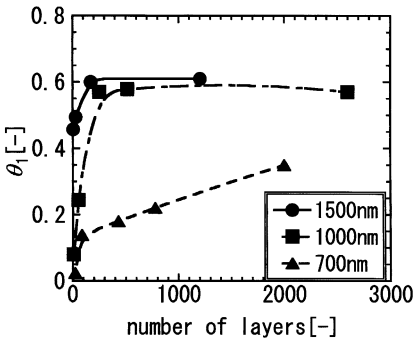

Figure 9. Relation between the filling factor and the number of the sedimentation layers.

however, the increase decelerated, as in the first layer, and the changes in the filling factor were smaller than those of the first layer, as shown in Figure 7b and 7d.

Figure 9 shows the relationship between the filling factor of the first layer on the substrate and the number of sedimentation layers. The number of sedimentation layers depends on the concentration of the silica suspensions with constant suspension volume. The filling factor increases as the number of sedimentation layers increases. When the diameter is 1,500 nm or 1,000 nm, the filling factor is saturated to a certain value of about 0.6. When the diameter is 700 nm, the saturation is not attained in this regard.

Discussion

Influence of pH and the drying process on the distance between the nearest silica spheres

As shown in Figure 3, the silica spheres are arranged hexagonally and maintain a uniform distance, which suggests that the silica spheres are separated by an electrostatic repulsive force. To clarify the influence of the interaction, the pH was controlled at 3.5, 7.0, or 10. As shown in Figure 10, the silica spheres are negatively charged when the pH is higher than 3.5 and the absolute value of the ζ-potential in the higher pH is larger than that in a lower pH. Although periodic peaks attributed to the hexagonal structure are seen in Figure 4a when the diameter is 1,500 nm and the pH is 3.5, they are smaller and less sharp than those given at a higher pH, as shown in Figure 4b and 4c. At pH 3.5, no peak is observed in

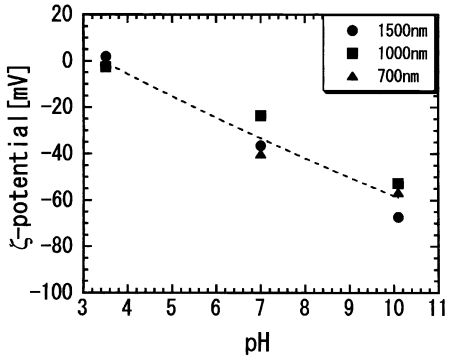

Figure 10. ζ-potential of silica spheres.

Figures 5a and 6a when the diameter is 1,000 nm and 700 nm. When the pH is 3.5, the silica spheres aggregate, and are not arranged into a hexagonal structure.

An electric double layer is formed on the surface of the silica spheres. The thickness of the electric double layer is represented by the Debye length, which is calculated to be 960 nm in a suspension at pH 7.0. It is, in fact, much smaller near the glass substrate (Crocker and Grier, 1996; Grier, 2000), because the electric double layer on the surface of the silica spheres in the first layer is affected by that of the glass substrate. When two particles approach within a Debye length, the overlap of the electric double layer causes a repulsive electrostatic interaction between the two particles. Apparently, a particle whose diameter is d behaves like a particle whose diameter is the effective diameter

$$d_{\text{eff}} = d + 2\kappa^{-1} \tag{4}$$

Moreover, the Debye length becomes larger at pH 10. As seen in Figure 4b and 4c, Figure 5b and 5c, and Figure 6b and 6c, however, the distance between the nearest two spheres at pH 7.0 is almost the same as that at pH 10, which means that the distance between the nearest two particles is not determined by the Debye length alone, but also by the electrostatic repulsive force from the upper layers. Figure 9 shows that the distance between the nearest two spheres is unique in each suspension concentration, which also suggests that the distance is affected by the electrostatic repulsive force from the upper layers.

Evaporation of water causes a capillary force by which silica spheres should approach each other. The distance to the nearest silica spheres is, however, larger than the diameter of the silica spheres. Thus, silica spheres would not be able to move freely and could not come into contact with each other.

Dynamics of the formation process of hexagonal arrays

In order to evaluate the dynamics of the formation process of the hexagonal arrays, we derive a rate equation for the formation process based on some assumptions. We assume that the increase in the filling factor of the first layer on the substrate at a certain time is proportional to the difference between the final filling factor and the filling factor at the time. This corresponds with the rate equation of the Langmuir-type adsorption, ignoring, the desorption part. The equation is written as below

$$\frac{d\theta_1}{dt} = k(\theta^* - \theta_1) \tag{5}$$

$$\frac{d}{dt}\left(\frac{\theta_1}{\theta^*}\right) = k\left(1 - \frac{\theta_1}{\theta^*}\right) \tag{6}$$

where k denotes the rate constant and θ^* denotes the final filling factor; and θ_1 denotes the filling factor of the first layer at $t = t$. In the early stage of sedimentation, the filling factor increases rapidly as the silica spheres precipitate, as shown in Figures 7. This increase in the filling factor is considered to be due to the silica spheres transported to the substrate by the spontaneous sedimentation. If each particle is dispersed and the electrostatic forces caused by other particles and the glass substrate are neglected, the increase in the filling factor is proportional to the number of silica spheres transported to the substrate, and the following boundary condition is derived at $t = 0$

$$\frac{d\theta_1}{dt} = \frac{\pi d^2 f}{4} \quad \text{at} \quad t = 0 \tag{7}$$

Since the suspensions in our study are not concentrated, the filling factor of the first layer before precipitation is zero

$$\theta_1 = 0 \quad \text{at} \quad t = 0 \tag{8}$$

From Eqs. 6–8, the filling factor of the first layer is given as a function of time

$$\frac{\theta_1}{\theta^*} = 1 - \exp(-kt) \quad \text{where} \quad k = \frac{\pi d^2 f}{4\theta^*} \tag{9}$$

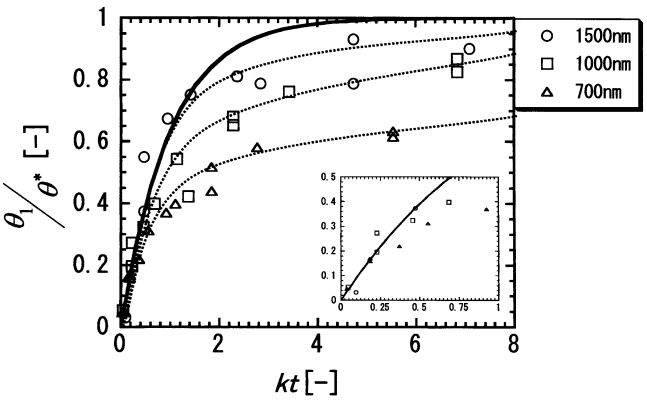

Figure 11. Data in Figure 7 determined by converting $\rho_1 - t$ to $\rho_1/\rho^* - kt$.

Calculated values based on Eq. 9 are shown as a solid line.

Data shown in Figure 7a–7d are repeated in Figure 11, converting a $\theta_1 - t$ plot to a $\theta_1/\theta^* - kt$ plot. θ^* is determined from Figure 9 where silica-sphere concentration is the highest. The filling factor is not saturated for 700 nm in Figure 9 despite being saturated for 1,500 nm and 1,000 nm, causing the final filling factor for 700 nm in Figure 11 to be overestimated. The solid line in Figure 11 shows the ratio of the filling factor of the first layer to the final filling factor calculated by Eq. 8. The filling factor given in the experiments in the early stage of the sedimentation agrees with the value calculated with the assumption, which confirms that the increase in the filling factor is caused by the transport of silica spheres by the spontaneous sedimentation, and the electrostatic forces caused by other particles and the glass substrate are negligible. Thus, it can be concluded that the rapid increase in the filling factor in the early stage of sedimentation is caused by the transport of the silica spheres by the spontaneous sedimentation. In the later stage of sedimentation, the changes in the filling factor with time, shown as dotted lines in Figure 11, is smaller than the calculation. This is due to the assumption that the rate constant is constant. In fact, the electrostatic repulsive force from the silica spheres of the first layer could decelerate the increase in the filling factor by preventing the subsequent spheres from entering the first layer.

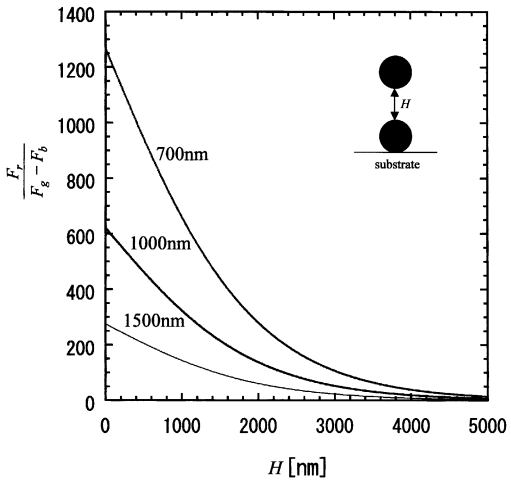

Figure 12. Calculated ratio of *Fr* to $(F_g - F_b)$.

The deviation of the calculated value from the experimental one of the filling factor is larger when the diameter is smaller. To explain the difference, we consider the forces attributed to a sphere precipitated to the first layer by simple DLVO theory, ignoring the effect of the glass substrate. We should consider the four forces, that is, the gravitational force, the buoyancy force, the frictional force from water, and the electrostatic repulsive force from other particles. The total force, F_{total}, is written as

$$F_{\text{total}} = F_g - F_b - F_f - F_{r,\text{total}} = \frac{\pi\rho_s g d^3}{6} - \frac{\pi\rho_w g d^3}{6} - 3\pi d\eta\nu - F_{r,\text{total}} \qquad (10)$$

where F_g, F_b, F_f, and $F_{r,\text{ total}}$ denote the gravitation force, the buoyancy force, the frictional force from water, and the electrostatic repulsive force from other particles, respectively. The total repulsive electrostatic force is given by the sum of the forces from others around a sphere. In a later stage of spontaneous sedimentation, the concentration of spheres in the first layer becomes larger than in the upper layer, and the total electrostatic repulsive force given to a sphere moving into the first layer is applied upward. The force causes a decrease in the sphere's velocity, as expected by Eq. 10. The decrease in the velocity is determined by the ratio of $F_{r,\text{ total}}$ to $(F_g\text{-}F_b)$. Now, for simplicity, two fixed spheres are considered. One is a sedimenting sphere in an upper layer, and the other is in the first layer vertically below (Figure 12). The electrostatic repulsive force, F_r, given to the upper sphere by the sphere in the first layer is written by the DLVO theory

$$F_r = \frac{\pi\epsilon d\psi_0^2 \exp\left(-\frac{H}{\kappa^{-1}}\right)}{\kappa^{-1}\left\{1+\exp\left(-\frac{H}{\kappa^{-1}}\right)\right\}} \qquad (11)$$

where ϵ, ψ_0, and H denote the dielectric constant of water, the surface potential of silica spheres, and the distance between the surface of two silica spheres, respectively; and κ^{-1} is the Debye length. The ratio of *Fr* to $(F_g\text{-}F_b)$ is shown in Figure 12. For simplicity, the Debye length in pure water, 960 nm, is adopted, and the average value of the measured ζ-potential at pH 7 shown in Figure 10 is approximately substituted for the surface potential in this calculation. As shown in Figure 12, the calculated F_r is more than hundreds to thousands of times as large as the calculated $(F_g\text{-}F_b)$. If the calculation overestimates the actual F_r, it would be due to an error in the surface potential and the Debye length given in the calculation. The calculated result is, however, qualitatively consistent with the experiments, where the electrostatic repulsive force is more effective in the case of smaller spheres, as shown in Figure 12.

As shown in Figure 8, the filling factors of the second layer on the substrate show a rapid increase early in the sedimentation stage, and a gradual increase in a later stage, as in the first layer. The changes in the filling factor of the second layer are slower than those of the first layer shown in Figure 7b and 7d. Since the deposition of the spheres in the second layer is followed by that in the first layer, there is a time lag in the second layer.

Formation mechanism of hexagonal arrays in spontaneous sedimentation

As shown in Figure 9, the filling factor increases with the increase in the number of upper layers. Since the first layer in each condition settles into hexagonal structure, the distance between the nearest silica spheres became smaller as the number of upper layers increased. The RDFs in Figure 4 also show a decrease in the distance between the nearest silica spheres from 450 s to 900 s. These results suggest a restructuring of the first layer by the precipitation of the upper layers. Figure 13 shows the scheme of the restructuring we expect. Silica spheres precipitate in the early stage, and the increase in the filling factor is due to the transport of the silica spheres by the spontaneous sedimentation, as described earlier. The silica spheres are gradually formed into hexagonal structures by the electrostatic repulsive force with a certain distance between them (Figure 13b). Figure 13(1) is a picture of when the number of layers is 2. In the later stage,

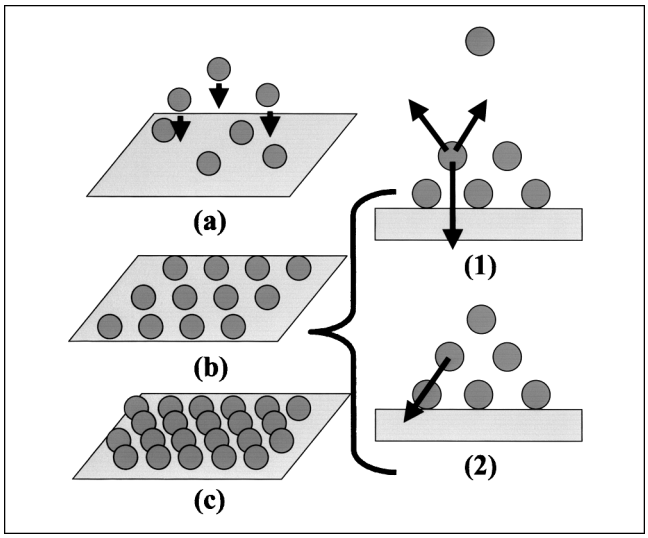

Figure 13. Formation process of three-dimensional arrays of silica spheres.

the silica spheres in the third layer are pushed down on the second layer by the electrostatic repulsive force (Figure 13(2)), and the spheres in the second layer are moved into the first layer, reducing the distance to the nearest spheres (Figure 13c). When the number of sedimentation layers is efficiently large, such as 1,000 or 10,000, the distance between the nearest two particles in the first layer is not decreased, because the electrostatic repulsive force against the second layer becomes greater preventing the spheres in the second layer from moving into the first layer.

Conclusion

In the spontaneous precipitation of silica spheres, the formation process of hexagonal arrays was directly observed by confocal laser scanning microscopy. Silica spheres are arranged into a hexagonal array, but do not come in contact with each other. The rate constant of the dynamics of the formation is attributed to the transport of the silica spheres in the early stage of the sedimentation, and it becomes smaller in the later stage. The distance between the nearest two spheres is not changed much by the pH, even if it is not near the isoelectric point. Based on the RDF and the change in the filling factor caused by the number of upper layers, the formation mechanism in the spontaneous sedimentation was deduced as shown in Figure 13.

From the results, in the condition of higher repulsive force at a higher pH, the distance from the nearest spheres is large, and the structure of the hexagonal arrays would be destroyed during the drying. While in the lower repulsive force state, when the pH is near the isoelectric point, spheres aggregate and do not form hexagonal structures.

To fabricate three-dimensional silica-sphere arrays with high regularity, the regular structure in the precipitation should be produced and structural change during the drying should be prevented. The surface state of the spheres should be optimized by controlling the pH, the surface potential, and so on, to make the distance between the nearest two spheres as small as possible while maintaining the hexagonal structure.

Acknowledgment

This work is financially supported by Grant-in-Aid for Scientific Research, JSPS, and the nanoparticle project, NEDO.

We are grateful to Dr. S. Maenosono and Prof. Y. Yamaguchi for their support and helpful advice. Mr. T. Shiraki and Dr. J. Plévert are acknowledged for providing the computer programs to illustrate the radial distribution function. Samples of silica spheres were provided by Nippon Shokubai Co., Ltd.

Notation

f = flux by number, spheres $m^{-2} \cdot s^{-1}$
C = number concentration, spheres m^{-3}
d = diameter of silica spheres, m
g = gravitational acceleration, $m \cdot s^{-2}$
N = number of circles drawn with silica spheres in unit area, spheres m^{-2}
d_{eff} = effective diameter, m
F_{total} = total force, N
F_g = gravitation force, N
F_b = buoyancy force, N
F_f = frictional force, N
$F_{r,total}$ = the total electrostatic respulsive force, N
F_r = electrostatic repulsive force between two spheres, N
H = distance between two silica spheres, m
k = rate constant, s^{-1}

Greek letters

ϵ = dielectric constant of water, $F \cdot m^{-1}$
η = viscosity of water, $Pa \cdot s$
θ = filling factor
θ_1 = filling factor of the first layer
θ_2 = filling factor of the second layer
θ^* = final filling factor

κ^{-1} = Debye length, m
ν = sedimentation velcoity, $m \cdot s^{-1}$
ρ_s = density of silica spheres, $kg \cdot m^{-3}$
ρ_w = density of water, $kg \cdot m^{-3}$
ψ_0 = surface potential of silica spheres, V

Literature Cited

Ackerson, B. J., and K. Schatzel, "Classical Growth of Hard-Sphere Colloidal Crystals," *Phys. Rev. E*, **52**, 6448 (1995).

Bogomolov, V. N, S. V. Gaponenko, I. N. Germanenko, A. M. Kapitonov, E. P. Petrov, N. V. Gaponenko, A. V. Prokofiev, A. N. Ponyavina, N. I. Silvanovich, and S. M. Samoilovich, "Photonic Band Gap Phenomenon and Optical Properties of Artificial Opals," *Phys. Rev. E*, **55**, 7619 (1997).

Crocker, J. C., and D. G. Grier, "When Like Charges Attract: The Effects of Geometrical Confinement on Long-Range Colloidal Interactions," *Phys. Rev. Lett.*, 77, 1897 (1996).

Denkov, N. D., O. D. Velev, P. A. Kralchevsky, I. B. Ivanov, H. Yoshimura, and K. Nagayama, "Mechanism of Formation of 2-Dimensional Crystals from Latex-Particles on Substrates," *Langmuir*, **8**, 3183 (1992).

Dimitrov, A. S., and K. Nagayama, "Continuous Convective Assembling of Fine Particles into Two-Dimensional Arrays on Solid Surfaces," *Langmuir*, **12**, 1303 (1996).

Grier, D. G., "When Like Charges Attract: Interactions and Dynamics in Charge-Stabilized Colloidal Suspensions," *J. Phys.: Condens. Matter*, **12**, A85 (2000).

Harland, J. L., and W. van Megen, "Crystallization Kinetics of Suspensions of Hard Colloidal Spheres," *Phys. Rev. E*, **55**, 3054 (1997).

Holgado, M., F. García-Santamaría, A. Blanco, M. Ibisate, A. Cintas, H. Míguez, C. J. Serna, C. Molpeceres, J. Requena, A. Mifsud, F. Meseguer, and C. López, "Electrophoretic Deposition to Control Artificial Opal Growth,' *Langmuir*, **15**, 4701 (1999).

Joannopoulos, J. D., R. D. Meade, and J. N. Winn, *Photonic Crystals*, Princeston Univ. Press, Princeton, NJ (1995).

John, S., "Strong Localization of Photons in Certain Disordered Dielectric Superlattices," *Phys. Rev. Lett.*, **58**, 2486 (1987).

Míguez, H., F. Meseguer, C. López, A. Mifsud, J. S. Moya, and L. Vázquez, "Evidence of FCC Crystallization of SiO_2 Nanospheres," *Langmuir*, **13**, 6009 (1997).

Park, S. H., D. Qin, and Y. Xia, "Crystallization of Mesoscale Particles over Large Areas," *Adv. Mater.*, **10**, 1028 (1998).

Pusey, P. N., and W. van Megen, "Phase-Behavior of Concentrated Suspensions of Nearly Hard Colloidal Spheres," *Nature*, **320**, 340 (1986).

Rogach, A. L., N. A. Kotov, D. S. Koktysh, J. W. Ostrander, and G. A. Ragoisha, "Electrophoretic Deposition of Latex-Based 3D Colloidal Photonic Crystals: A Technique for Rapid Production of High-Quality Opals," *Chem. Mater.*, **12**, 2721 (2000).

Xia, Y., B. Gates, Y. Yin, and Y. Lu, "Monodispersed Colloidal Spheres: Old Materials with New Applications," *Adv. Mater.*, **12**, 693 (2000).

Yablonovitch, E., "Inhibited Spontaneous Emission in Solid-State Physics and Electronics," *Phys. Rev. Lett.*, **58**, 2059 (1987).

Yoshida, H, K. Ito, and N. Ise, "Colloidal Crystal-Growth," *J. Chem. Soc. Faraday Trans.*, **87**, 371 (1991).

Manuscript received June 28, 2002, and revision received Oct. 17, 2002.